

Experimental and theoretical multichannel study of direct nuclear reactions: a tool to provide data driven information on neutrino-less double-beta decay

Alessandro Spatafora^{1,}, Diana Carbone¹, Francesco Cappuzzello^{2,1}, Manuela Cavallaro¹, Luis E. Acosta³, Clementina Agodi¹, Paulina Amador-Valenzuela⁴, Thereza Borello-Lewin⁵, Giuseppe A. Brischetto¹, Daniela Calvo⁶, Efrain R. Chávez-Lomeli³, Irene Ciraldo¹, Giovanni De Gregorio^{7,8}, Franck Delaunay^{1,2,9}, Haris Djapo¹⁰, Canel Eke¹¹, Paolo Finocchiaro¹, Suna Firat¹², Maria Fisichella¹, Angela Gargano⁹, Aylin Hacisalihoglu¹³, José A. Lay^{14,15}, Roberto Linares¹⁶, Jesus Lubian¹⁶, Nilberto Medina¹⁷, Mauricio Morales¹⁷, José R. B. Oliveira⁵, Athena Pakou¹⁸, Luciano Pandola¹, Horia Petrascu¹⁹, Onoufrios Sgouros¹, Marcelli A. G. da Silveira²⁰, Selçuk O. Solakci¹², Vasilis Soukeras¹, George A. Souliotis²¹, Domenico Torresi¹, Salvatore Tudisco¹, Aydin Yıldırım¹², and Vinicius A. B. Zagatto⁵*

¹Istituto Nazionale di Fisica Nucleare, Laboratori Nazionali del Sud, Catania, Italy

²Dipartimento di Fisica e Astronomia, Università di Catania, Catania, Italy

³Instituto de Física, Universidad Nacional Autónoma de México, México City, México

⁴Instituto Nacional de Investigaciones Nucleares, Ocoyoacac, México

⁵Instituto de Física, Universidade de São Paulo, São Paulo, Brazil

⁶Istituto Nazionale di Fisica Nucleare, Sezione di Torino, Torino, Italy

⁷Istituto Nazionale di Fisica Nucleare, Sezione di Napoli, Napoli, Italy

⁸Dipartimento di Matematica e Fisica, Università della Campania, Caserta, Italy

⁹LPC Caen UMR6534, Université de Caen Normandie, ENSICAEN, CNRS/IN2P3, Caen, France

¹⁰Ankara University, Institute of Accelerator Technologies, Turkey

¹¹Department of Mathematics and Science Education, Akdeniz University, Antalya, Turkey

¹²Department of Physics, Akdeniz University, Antalya, Turkey

¹³Institute of Natural Science, Karadeniz Teknik Üniversitesi, Trabzon, Turkey

¹⁴Departamento de FAMN, University of Seville, Spain

¹⁵Instituto Carlos I de Física Teórica y Computacional, University of Seville, Spain

¹⁶Instituto de Física, Universidade Federal Fluminense, Niterói, Brazil

¹⁷Instituto de Pesquisas Energeticas e Nucleares, São Paulo, Brazil

¹⁸Department of Physics, University of Ioannina and Hellenic Institute of Nuclear Physics, Ioannina, Greece

¹⁹Horia Hulubei National Institute for R&D in Physics and Nuclear Engineering, Magurele, Romania

²⁰Centro Universitario FEI, São Bernardo do Campo, Brazil

²¹Department of Chemistry, University of Athens and Hellenic Institute of Nuclear Physics, Athens, Greece

Abstract. The search for neutrino-less double beta decay has attracted much interest in the last years due to the extraordinary consequences that could derive from its observation. In the view to provide experimental information on the nuclear matrix elements involved in the expression of neutrino-less double

*e-mail: alessandro.spatafora@lns.infn.it

beta decay half-life, the NUMEN project is measuring cross-sections of double charge exchange and other quasi-elastic nuclear reactions using the MAGNEX magnetic spectrometer. In particular, the newly proposed multichannel approach, applied both to the experimental and theoretical analysis, will be discussed.

1 Introduction and motivation

Neutrino-less double-beta decay ($0\nu\beta\beta$) is considered the *experimentum crucis* to reveal the Majorana nature of neutrinos and the lepton-number violation, being a link between the current and next-generation physics beyond the standard model [1]. The role of nuclear matrix elements (NMEs) in $0\nu\beta\beta$ research is crucial to design the next-generation experiments and to access the neutrino effective mass, if the process will be actually observed [2]. Due to that, the present spread in the results of about a factor of three for the NMEs calculated among different nuclear structure theories need to be overcome [3]. In order to constraint the NMEs values, experiments adopting a broad variety of nuclear probes have been performed in the past decades [2]. Although interesting, all these measurements revealed to be still not conclusive for the $0\nu\beta\beta$ -decay NMEs.

Heavy-ion Double Charge Exchange (HI-DCE) studies have been recently proposed to stimulate the same g.s. to g.s. transition occurring in the $0\nu\beta\beta$ -decay and to access the nuclear response to the second order isospin operator, in analogy to the $0\nu\beta\beta$ -decay second order weak process. This analogy is the *leitmotiv* of the NUMEN (Nuclear Matrix Elements for neutrino-less double-beta decay) and NURE projects [4–8]. Promising results regarding the possibility to extract the DCE NME from the experimental cross-section measurements have been achieved in the last few years [9]. DCE reactions are characterized by the transfer of two units of charge, leaving the mass number unchanged, and can proceed by a sequential nucleon-transfer mechanism or by exchange of two isovector mesons, in an uncorrelated or correlated way. Despite $0\nu\beta\beta$ decays and HI-DCE are mediated by different interactions, they share a number of similarities. The key aspect is that initial and final nuclear states are the same and the transition operators are made by a short-range isospin, spin-isospin and rank-two tensor components with a relevant available momentum (100 MeV/c or so). In addition, NUMEN aims at the exploration of all the relevant reaction channels populated in the projectile/target interaction, including the elastic and inelastic scattering, one and two nucleon transfer, and single charge exchange (SCE) reactions.

The NUMEN project aims to study the ($^{18}\text{O}, ^{18}\text{Ne}$) DCE reaction as a probe for the $\beta^+\beta^+$ transitions and the ($^{20}\text{Ne}, ^{20}\text{O}$) and the ($^{12}\text{C}, ^{12}\text{Be}$) DCE reactions for the $\beta^-\beta^-$ one, to explore the DCE mechanisms in both directions for all the $0\nu\beta\beta$ candidates [7, 9]. Since NMEs are *time invariant* quantities, they are common to a DCE and to its inverse, so that the contextual measurements of both directions in the DCE are a useful way to test the capability to properly extract the NME from the measured DCE cross-section. NUMEN is conceived in a long-range time perspective, in the view of a comprehensive study of many candidate systems for $0\nu\beta\beta$ decay. Moreover, the project has promoted a renewal of the INFN-LNS research infrastructure and a specific R&D activity on detectors, materials and instrumentation [4]. The NUMEN experimental campaign, conducted so far at INFN-LNS using the K800 Superconducting Cyclotron and the MAGNEX large acceptance magnetic spectrometer [10], have brought to first results giving encouraging indication on the capability of the proposed technique to access relevant quantitative information.

2 The DCE reaction mechanism and the multichannel approach

The hard task to extract the NMEs from the DCE cross-section measurements could be accomplished provided that the complete description of the DCE reaction mechanism is completely under control [9]. The description of the complete nuclear reaction mechanism of DCE needs a formulation based on quantum-mechanical microscopic reaction theory which accounts for the possible competition of different processes feeding the DCE channel. The three main reaction mechanisms competing in the full DCE process are: the Majorana-DCE (MDCE), the double-Single Charge-Exchange (DSCE) and the multi-nucleon transfer-DCE (TDCE). The TDCE mechanism can be described within distorted wave Born approximation (DWBA) or coupled channels methods. However, the practical implementation of a sufficiently complete calculation has not been possible until very recent times [11], due to the fact that at least fourth order nucleon transfer schemes are required. For DSCE, the theoretical framework formerly introduced for SCE by Lenske et al. [12], has been recently extended to second order [13, 14]. In this process, the successive exchange of two uncorrelated charged mesons is taken into account. This formalism reveals a remarkable similarity of DSCE with $2\nu\beta\beta$ decay, although a much richer multipole spectrum is accessed in HI-DCE. A completely new reaction mechanism, named Majorana mechanism (MDCE), has been recently introduced in Refs. [9, 15]. The MDCE mechanism relies on neutral mesons induced nucleon-nucleon short range correlations. The included correlations bring to a single step reaction mechanism and suggest an intriguing connection of this formalism with $0\nu\beta\beta$.

As a typical feature of direct reactions, DCE cross sections critically depend on the ion-ion initial and final state interaction and represent a minor component of the outgoing flux in heavy-ion collisions [16]. In addition, the coupling between a specific reaction channel and the elastic channel and other direct processes makes it necessary to study all of them in a comprehensive approach. From the experimental side, all the different reaction cross sections should be measured under the same laboratory conditions. From the theory side, a high consistency is required in order to simultaneously describe the different degrees of freedom, selectively activated by the various direct reactions, in the same microscopic approach. A clear advantage of the multichannel approach is the possibility to use a broad and correlated ensemble of experimental data in the analyses, thus reducing the need of free parameters in the adopted theoretical models. On the other hand, such a requirement demands for sophisticated data analyses, where different reaction channels are studied in the same context. The actual implementation of such a multichannel approach has been rarely used in the analyses of data, mainly due to the complexity of the problem from both the experimental and the theoretical side. For such reasons the NUMEN project proposed, and is actually adopting, a multichannel approach, in which a wide network of reaction channels is under study. The network includes the elastic and inelastic scattering [17–20], the one- and two-nucleon transfer [21–27], the SCE [28–30] and DCE [10, 31] reaction channels.

In the next section, the method is applied to the study of the $^{18}\text{O} + ^{12}\text{C}$ system at 275 MeV incident energy. Although they are not $\beta\beta$ -decay candidates, the choice of such projectile and target was driven by the available accurate information on the involved low-lying nuclear states in this mass region from experimental results and large scale shell-model calculations, making this system an ideal benchmark for the proposed multichannel constrained technique. The newly proposed multichannel technique is supposed to be applied to the study of the $\beta\beta$ -decay candidates. The extraction of new experimental data and the theoretical analysis relating to them are ongoing for the networks of nuclear reactions involving the $^{76}\text{Ge} \leftrightarrow ^{76}\text{Se}$ $\beta\beta$ -decay partners. In particular, preliminary results will be discussed in the last section in the case of the elastic and inelastic scattering, the SCE and the DCE nuclear reaction channels. New preliminary SCE spectra will be presented for the first time.

3 The $^{18}\text{O} + ^{12}\text{C}$ test-benchmark nuclear reaction

The study of the $^{18}\text{O} + ^{12}\text{C}$ system at 275 MeV incident energy was chosen as an ideal benchmark to test the possibility to separate, using the multichannel technique, the nuclear reaction from the nuclear structure features of the nuclei involved in the reaction. The experiment was performed at INFN-LNS [32] where the ^{18}O beam was accelerated up to 275 MeV by the K800 Superconducting Cyclotron. The $60 \pm 3 \mu\text{g}/\text{cm}^2$ and the $200 \pm 10 \mu\text{g}/\text{cm}^2$ thick ^{nat}C self-supporting targets were located in the object point of the MAGNEX magnetic spectrometer [33]. A Faraday cup and an electron suppressor were used to stop the beam and collect the charge with a collection accuracy better than 10% in all the experimental runs. The MAGNEX optical axis was oriented, compared to the beam direction, at $\theta_{opt} = 7.5^\circ, 8^\circ$ and 13.5° . The magnetic fields of the dipole and quadrupole magnets were set in order to transport the $^{18}\text{F}^{9+}, ^{19}\text{F}^{9+}, ^{17}\text{O}^{8+}$ and $^{16}\text{O}^{8+}$ ions corresponding to the ejectiles of the nuclear reactions of interest in the region of momenta covered by the MAGNEX focal plane detector (FPD) [34]. The study of the elastic and inelastic scattering was performed in a different magnetic set since the magnetic rigidity of the $^{18}\text{O}^{8+}$ is too different with respect to the ones of the other ions to be detected in the same magnetic set. The data reduction strategy includes the position calibration of the FPD, identification of the ejectiles and reconstruction of the momentum vector at the target by inversion of the transport equations following the guidelines presented in previous publications [35, 36].

The elastic and inelastic scattering, one-proton stripping, one-neutron pick-up and SCE nuclear reaction excitation energy spectra were previously published in Refs. [37–39]. An example from Ref. [39] is shown in Fig. 1. The excitation energy E_x was calculated as the difference $Q_0 - Q$ where the Q_0 is the ground-to-ground state Q -value and Q is the Q -value obtained by the missing-mass technique based on relativistic kinematic transformations. The energy resolution (≈ 0.6 MeV) is slightly dependent on the reaction channel due to the different energy straggling produced by the ejectile/target interaction. The achieved energy resolution was enough to single out transitions to isolated or grouped states of the residual nuclei. Absolute cross-section angular distributions were extracted for the several structures clearly visible in the spectra. Theoretical analysis for the elastic and inelastic scattering, one-proton stripping, one-neutron pick-up are published in Ref. [39] while the complete analysis of the SCE reaction channel mechanism will be published in forthcoming publications.

4 Study of the ^{76}Ge $0\nu\beta\beta$ -decay candidate

The new multichannel experimental and theoretical approach was applied to a wide network of nuclear reactions involving the ^{76}Ge and ^{76}Se $\beta\beta$ decay partners. Two experiments were dedicated to this scope and many nuclear reaction channels were studied, including the $^{76}\text{Ge} \leftrightarrow ^{76}\text{Se}$ transition populated in both directions through the $(^{18}\text{O}, ^{18}\text{Ne})$ and the $(^{20}\text{Ne}, ^{20}\text{O})$ DCE reactions.

The $^{18}\text{O} + ^{76}\text{Se}$ and the $^{20}\text{Ne} + ^{76}\text{Ge}$ collisions at 15.3 AMeV incident energy were performed at the LNS-INFN using the $^{18}\text{O}^{8+}$ and the $^{20}\text{Ne}^{10+}$ beams accelerated by the K800 Superconducting Cyclotron. The beam ions impinged on the ^{76}Se and ^{76}Ge targets evaporated on ^{nat}C backing layers and located in the object point of the MAGNEX magnetic spectrometer [33, 36, 40, 41], inside its scattering chamber. The ejectiles were momentum analysed in different runs in which the optical axis of MAGNEX was oriented, compared to the beam direction, at several θ_{opt} angles. During the $^{76}\text{Se}(^{18}\text{O}, ^{18}\text{Ne})^{76}\text{Ge}$ and the $^{76}\text{Ge}(^{20}\text{Ne}, ^{20}\text{O})^{76}\text{Se}$ DCE reaction cross-section measurements, the MAGNEX spectrometer was placed at $\theta_{opt} = +3^\circ$ and -3° , respectively, including zero degree in the full acceptance mode (≈ 50 msr), and the total covered angular range was $0^\circ \leq \theta_{lab} \leq 9^\circ$. In these configurations, the beam enters

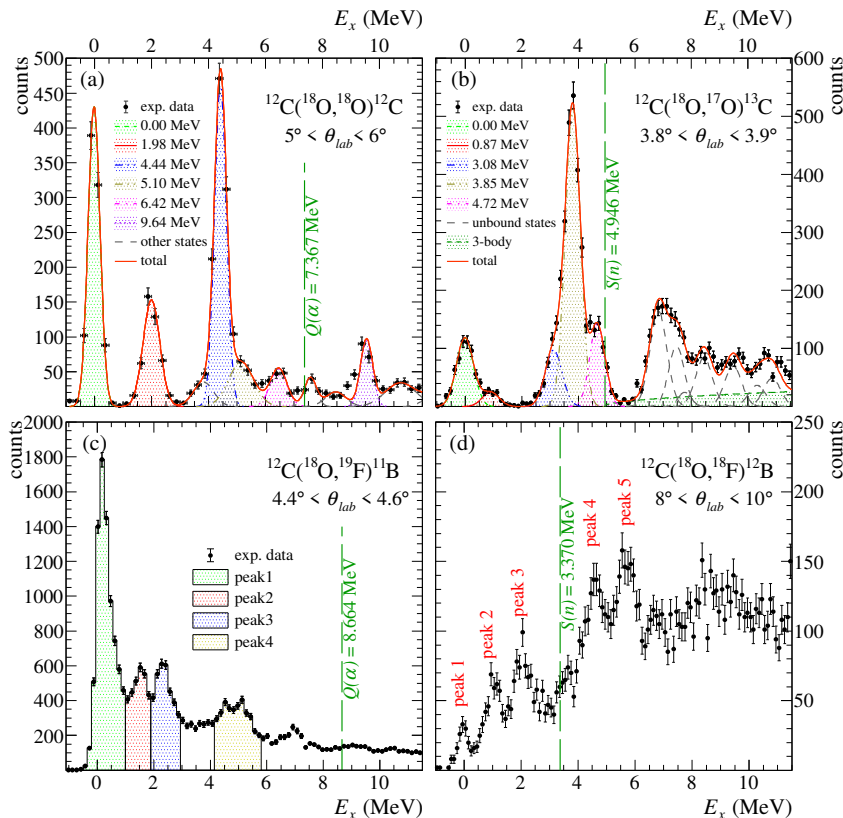


Figure 1. Excitation energy spectra for the net of nuclear reactions involved in the multichannel study of the SCE reactions coming from the $^{18}\text{O} + ^{12}\text{C}$ collision at 275 MeV incident energy. (a) $^{12}\text{C}(^{18}\text{O}, ^{18}\text{O})^{12}\text{C}$ elastic and inelastic scattering energy spectrum at $5^\circ < \theta_{lab} < 6^\circ$. Lines, obtained from best-fit procedure, identify peaks corresponding to the superposition of the projectile and target states, as labeled in the legend. (b) $^{12}\text{C}(^{18}\text{O}, ^{17}\text{O})^{13}\text{C}$ one-neutron stripping energy spectrum at $3.8^\circ < \theta_{lab} < 3.9^\circ$. Lines, obtained from best-fit procedure, identify peaks corresponding to the superposition of the projectile and target states, as labeled in the legend. (c) $^{12}\text{C}(^{18}\text{O}, ^{19}\text{F})^{11}\text{B}$ one-proton pick-up energy spectrum at $4.4^\circ < \theta_{lab} < 4.6^\circ$. The hatched areas indicate the regions of interest for the study of the angular distributions as labeled in the legend. (d) $^{12}\text{C}(^{18}\text{O}, ^{18}\text{F})^{12}\text{Be}$ SCE energy spectrum at $8^\circ < \theta_{lab} < 10^\circ$. Figure from Ref. [39].

in the spectrometer acceptance and the magnetic fields guide it to a place in the focal plane region away from the detectors [42]. A Faraday cup of 0.8 cm entrance diameter and 3 cm depth, mounted 15 cm downstream of the target, was used to stop the beam and collect the charge during the non-zero degree measurements. An electron suppressor polarized at -200 V and a low noise charge integrator allowed to keep the charge collection accuracy better than 10% in all the experimental runs.

The beam current was optimized at each optical angle configuration in order to reach event rates tolerable by the focal plane detector (FPD) [34]. The magnetic fields of the dipole and quadrupole magnets were set in order to transport the ions of interest in the region of momenta covered by the FPD. The data reduction strategy includes the position calibration

Table 1. Main parameters characterizing the experimental set-up of each explored reaction channel: target, and carbon backing thicknesses, covered scattering angles $[\theta_{lab}^{min}; \theta_{lab}^{max}]$, MAGNEX central angle θ_{opt} , magnetic rigidity $B\rho$, quadrupole field BQ and MAGNEX solid angle acceptance are given.

	target ($\mu\text{g}/\text{cm}^2$)	C backing ($\mu\text{g}/\text{cm}^2$)	$[\theta_{lab}^{min}; \theta_{lab}^{max}]$ (deg)	θ_{opt} (deg)	$B\rho$ (Tm)	BQ (T)	Ω (msr)
$^{76}\text{Se}(^{18}\text{O}, ^{18}\text{O})^{76}\text{Se}$	280 ± 15	80 ± 4	$[3.0; 18.5]$	8.0			49.2
				8.0	1.1968	-0.6638	35.0
				14.0			49.2
				18.0			49.2
$^{76}\text{Se}(^{18}\text{O}, ^{18}\text{F})^{76}\text{As}$	280 ± 15	80 ± 4	$[3.0; 14.0]$	8.0	1.1495	-0.6220	13.6
$^{76}\text{Se}(^{18}\text{O}, ^{18}\text{Ne})^{76}\text{Ge}$	280 ± 15	80 ± 4	$[0.0; 9.0]$	3.0	1.0086	-0.5482	10.4
$^{76}\text{Ge}(^{20}\text{Ne}, ^{20}\text{Ne})^{76}\text{Ge}$	390 ± 20	56 ± 3	$[3.0; 20.0]$	8.0			49.2
				8.0	1.1397	-0.6805	32.0
				13.0			49.2
				16.0			49.2
				19.0			49.2
$^{76}\text{Ge}(^{20}\text{Ne}, ^{20}\text{F})^{76}\text{As}$	390 ± 20	56 ± 3	$[3.0; 14.0]$	8.0	1.2270	-0.6286	1.6
$^{76}\text{Ge}(^{20}\text{Ne}, ^{20}\text{O})^{76}\text{Se}$	390 ± 20	56 ± 3	$[0.0; 9.0]$	-3.0	1.3761	-0.8175	49.2

of the FPD, identification of the ejectiles and reconstruction of the momentum vector at the target by inversion of the transport equations following the guidelines presented in previous publications [35]. Target thicknesses, covered scattering angles, spectrometer optical angles and explored solid angles are listed in Table 1 for each of the presented reaction channels.

The accurate set-up and the advanced data reduction have allowed to produce high resolution energy spectra and angular distributions for all the analysed channels. The excitation energy E_x was calculated as the difference $Q_0 - Q$ where the Q_0 is the ground to ground state Q -value and Q is the Q -value obtained by the missing mass technique based on relativistic kinematic transformations. E_x measured spectra are shown in Figs. 1 of Refs. [18] and [20] for the $^{18}\text{O} + ^{76}\text{Se}$ and $^{20}\text{Ne} + ^{76}\text{Ge}$ elastic and inelastic scattering at 15.3 AMeV, respectively. In these cases, the achieved energy resolution is about 0.5 MeV. Slightly better values are obtained for the other reaction channels, depending on the different energy straggling produced by the ejectile/target interaction.

The results of the study on the $^{76}\text{Se}(^{18}\text{O}, ^{18}\text{O})^{76}\text{Se}$ and $^{76}\text{Ge}(^{20}\text{Ne}, ^{20}\text{Ne})^{76}\text{Ge}$ elastic and inelastic scattering were published in Refs. [18] and [20] and discussed during the conference. Preliminary results on the zero-degree $^{76}\text{Se}(^{18}\text{O}, ^{18}\text{Ne})^{76}\text{Ge}$ and the $^{76}\text{Ge}(^{20}\text{Ne}, ^{20}\text{O})^{76}\text{Se}$ DCE cross-sections measurements were also presented, although further theoretical investigations are needed in order to master the difficult matter of extracting a nuclear matrix element.

The preliminary ^{76}As spectra populated in the new $(^{18}\text{O}, ^{18}\text{F})$ and $(^{20}\text{Ne}, ^{20}\text{F})$ heavy-ion SCE reactions' measurements are shown in Figure 2. The former is more structured than the latter, due to a possible concentration of the SCE transition strength in a smaller number of states. A similar comparison was carried out in the past using the $(\text{d}, ^2\text{He})$ and $(^3\text{He}, \text{t})$ from Refs. [43] and [44] spectra. In these cases, the authors concluded that while from the $^{76}\text{Se} \rightarrow ^{76}\text{As}$ side the GT strength is almost concentrated in few states, from the $^{76}\text{Ge} \rightarrow ^{76}\text{As}$ one the GT strength is much more fragmented. Our work is extending this result up to larger transferred momenta, only accessible via heavy-ion induced SCE reactions. Absolute cross-section angular distributions were extracted for the several structures clearly visible in the spectra and, as previously mentioned, the theoretical analysis of these important results is still ongoing and their publication process is in progress.

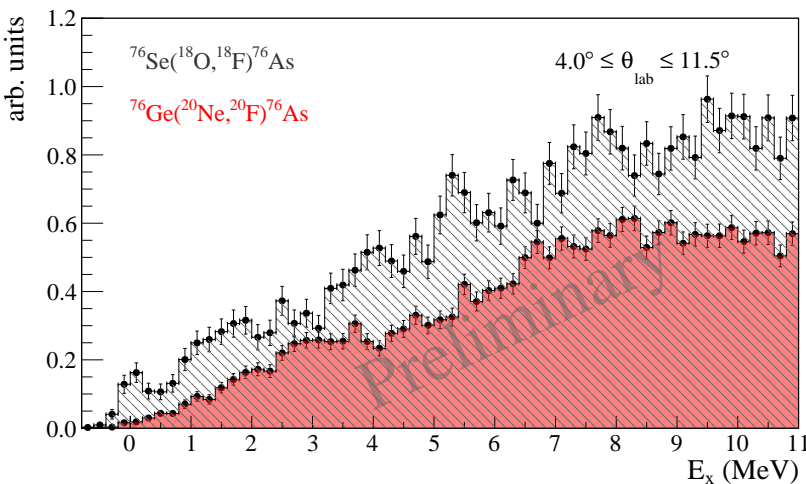


Figure 2. Superposition of the ^{76}As excitation energy spectra obtained from the $^{76}\text{Se}(^{18}\text{O}, ^{18}\text{F})^{76}\text{As}$ (black hatched) and $^{76}\text{Ge}(^{20}\text{Ne}, ^{20}\text{F})^{76}\text{As}$ (red filled) single charge-exchange nuclear reactions at 15.3 AMeV incident energy and $4^\circ \leq \theta_{lab} \leq 11.5^\circ$.

Acknowledgments

This project received funding from the European Research Council (ERC) under the European Union's Horizon 2020 research and innovation program (Grant Agreement No. 714625).

References

- [1] M.J. Dolinski et al., Annual Review of Nuclear and Particle Science **69**, 219 (2019)
- [2] H. Ejiri, J. Suhonen, K. Zuber, Physics Reports **797**, 1 (2019)
- [3] M. Agostini et al., Rev. Mod. Phys. **95**, 025002 (2023)
- [4] F. Cappuzzello et al., Int. Jour. of Mod. Phys. A **36**, 2130018 (2021)
- [5] F. Cappuzzello et al., Frontiers in Astronomy and Space Sciences **8**, 668587 (2021)
- [6] P. Finocchiaro et al., Universe **6**, 129 (2020)
- [7] F. Cappuzzello et al., European Physical Journal A **54**, 72 (2018)
- [8] M. Cavallaro et al., PoS BORMIO2017 **015** (2017)
- [9] F. Cappuzzello et al., Prog. in Part. and Nucl. Phys. **128**, 103999 (2023)
- [10] F. Cappuzzello et al., Eur. Phys. J. A **51**, 145 (2015)
- [11] J. Ferreira et al., Physical Review C **105** (2022)
- [12] H. Lenske et al., Progress in Particle and Nuclear Physics **109**, 103716 (2019)
- [13] J.I. Bellone et al., Physics Letters, Section B: Nuclear, Elementary Particle and High-Energy Physics **807** (2020)
- [14] H. Lenske et al., Universe **7** (2021)
- [15] H. Lenske, J. Phys.: Conf. Ser. **1056**, 012030 (2018)
- [16] H. Lenske et al., Universe **10**, 2 (2024)
- [17] G. Brischetto et al., Physical Review C **109** (2024)

- [18] L. La Fauci et al., *Phys. Rev. C* **104**, 054610 (2021)
- [19] D. Carbone et al., *Universe* **7**, 58 (2021)
- [20] A. Spatafora et al., *Phys. Rev. C* **100**, 034620 (2019)
- [21] I. Ciraldo et al., *Physical Review C* **109** (2024)
- [22] O. Sgouros et al., *Physical Review C* **108** (2023)
- [23] I. Ciraldo et al., *Phys. Rev. C* **105**, 044607 (2022)
- [24] O. Sgouros et al., *Phys. Rev. C* **104**, 034617 (2021)
- [25] S. Calabrese et al., *Phys. Rev. C* **104**, 064609 (2021)
- [26] J.L. Ferreira et al., *Phys. Rev. C* **103**, 054604 (2021)
- [27] D. Carbone et al., *Physical Review C* **102**, 044606 (2020)
- [28] B. Urazbekov et al., *Physical Review C* **108** (2023)
- [29] S. Burrello et al., *Phys. Rev. C* **105**, 024616 (2022)
- [30] M. Cavallaro et al., *Frontiers in Astronomy and Space Sciences* **8**, 61 (2021)
- [31] V. Soukeras et al., *Results in Physics* **28**, 104691 (2021)
- [32] *INFN-LNS web site*, <https://www.lns.infn.it/>
- [33] F. Cappuzzello, C. Agodi, D. Carbone, M. Cavallaro, *Eur. Phys. J. A* **52**, 167 (2016)
- [34] D. Torresi et al., *Nucl. Instr. and Meth. A* **989**, 164918 (2021)
- [35] D. Carbone, *The European Physical Journal Plus* **130**, 143 (2015)
- [36] M. Cavallaro et al., *Nucl.Instr.and Meth.A* **463**, 334 – 338 (2020)
- [37] A. Spatafora, *Nuovo Cimento della Societa Italiana di Fisica C* **45** (2022)
- [38] A. Spatafora et al., *Journal of Physics: Conference Series* **2453** (2023)
- [39] A. Spatafora et al., *Physical Review C* **107** (2023)
- [40] S. Calabrese et al., *Nucl. Instr. and Meth. A* **980**, 164500 (2020)
- [41] S. Calabrese et al., *Acta Phys. Polon. B* **49**, 275 (2018)
- [42] M. Cavallaro et al., *Res. in Phys.* **13**, 102191 (2019)
- [43] E.W. Grewe et al., *Phys. Rev. C* **78**, 044301 (2008)
- [44] J.H. Thies et al., *Phys. Rev. C* **86**, 014304 (2012)